DOI: 10.21062/mft.2023.016 http://www.journalmt.com

Influence of the Mn Content on the Corrosion Behaviour of HEA CoCrFeNiMnX (X=5, 20, 35 at.%) Prepared via MA+SPS

Filip Průša (0000-0002-6494-5084)[1], Petr Kratochvíl (0000-0002-1720-4646)[1], Hana Thürlová (0000-0001-7011-5573)[1], Darya Rudomilova (0000-0002-9269-2803)[2], Šárka Msallamová (0000-0002-3539-9897)[1]
[1]University of Chemistry and Technology Prague, Department of Metals and Corrosion Engineering Technická 5, 166 28 Prague 6, Czech Republic. *Email: filip.prusa@vscht.cz
[2]Technopark Kralupy, University of Chemistry and Technology Prague, 166 28 Prague, Czech Republic

The high entropy alloys with intended chemical compositions of CoCrFeNiMnX (X=5, 20 and 35 at.%) were prepared by the means of mechanical alloying. Prepared powders were then compacted using the progressive spark plasma sintering, which minimizes the deleterious microstructural coarsening. The compacts were, regardless of the actual chemical composition, composed of a solid solution with FCC crystallographic lattice and a small amount of carbides identified as Cr_7C_3. The dimensions of those carbides increased with the content of Mn, which was confirmed also by atomic force microscopy (AFM) and scanning kelvin probe microscopy (SKPM). The surface topography measured by AFM confirmed its presence as they emerged from the surface, perfectly matching the positive potential measured by the SKPM. It was found, that the HEAs are showing rather worse corrosion resistance in the aqueous environment containing 9 g/1 NaCl compared to the reference 316L stainless steel. Moreover, the higher the content of Mn, the worse the corrosion resistance increasing the corrosion current density and shifting open circuit potential towards more negative values. When exposed to the elevated temperature of 600 °C, the alloys formed a poor protective oxidic layer that tended to chip off due to thermal stresses.

Keywords: High entropy alloys, mechanical alloying, spark plasma sintering, potentiodynamic measurements, properties.

1 Introduction

Since 2004, High-entropy alloys (HEAs) became a fast-developing branch of contemporary research focused on a brand new type of materials offering usually an extraordinary combination of properties. Usually, five-element alloys are known for their high entropy of mixing favouring the preferential formation of solid solutions or their mixture with strengthening phases such as Laves phases or intermetallics. The crystallographic lattice of the solid solution is usually determining the resulting properties, namely the ductility, which is usually associated mainly with the FCC lattice. Therefore, the optimal combination of sufficient ductility while exhibiting good strengths is of the main research interest. This can be achieved due to microstructural refinement, e.g. by powder metallurgy techniques, such as rapid solidification[1], or via homogeneously dispersed particles.

Mechanical alloying is a highly promising method that combines both the aforementioned approaches providing a well-refined microstructure together with finely dispersed reinforcing particles. On top of that, it significantly improves the mechanical properties due to the intensive deformation increasing the concentration of lattice defects. More importantly, the use of a Process Control Agent (PCA) in form of different organic compounds is known to be responsible for the enrichment of the prepared alloy by C that is capable to form carbides. This happens via in-situ reactions during the consequential compaction via SPS. This behaviour has been reported also in previous works [1-6], among which the direct contact of the alloy with the graphite die walls is also having a significant role. However, as we are aware, the carbides are homogeneously dispersed throughout the entire cross-section of the compacted alloy favouring the origin of C contamination arising from the PCA.

The CoCrFeNiMn alloy belongs to the most widely investigated, although it has been almost exclusively prepared either by induction casting or by arc-melting methods, both generating rather coarse-grained microstructures, showing significant heterogeneity. On the other hand, mechanical alloying is fairly used for the preparation of HEAs, except in some of our previous works [2-5, 7]. Among that, the corrosion resistance, either in the aqueous or dry environment, has been largely overlooked. There are only a few scientific reports describing such features, even for the well-known CoCrFeNiMn alloy. Considering the aqueous corrosion, the situation is even more disturbing since these reports are focused

on materials/layers prepared by significantly different methods, such as laser cladding [8], and arc melting [9], while only one publication [10] is devoted to the CoCrFeNiMn alloy deposed as a layer via mechanical alloying. Considering the ability of HEAs to fine-tune the properties just by changing the content of particular elements, they might become highly universal materials, that can be either used as materials for implants or as structural materials for extreme conditions.

Therefore, the present manuscript is describing the basic behaviour of this alloy in A physiological solution representing the aqueous corrosion and in the dry environment to determine their high-temperature oxidation resistance. Moreover, the aqueous testing describes the influence of Mn content on these properties and compares them with 316L steel, which is commonly used for implants.

2 Experimental details

The CoCrFeNiMn HEAs with different content of Mn ranging from 5 – 35 at.%, were prepared using mechanical alloying and compacted via spark plasma sintering. Mechanical alloying was done in a milling jar filled with milling balls, both made of AISI 420 stainless steel. Elements used for the preparation of the alloys were used in a frame of similar powder particle dimensions. Therefore, we used the commercially available elements, namely Co (2 μm, 99.8 %), Cr (44 μm, ≥ 99.0 %), Fe (5-9 μm, 99.9 %), Ni (10 μm, 99.5 %) and Mn (≤ 10 μm, 99.6 %). From these powders, the Cr was the only one with powder particle sizes approximately four times larger. The appropriate amount of each pure element was placed into the milling jar together with 4 wt.% of n-heptane preventing excessive cold-welding. Then, the jar was sealed and flushed with a 99.995% Ar to prevent any oxidation during this preparation step. The weight ratio of the powder-to-balls was 15:1, and the alloying itself was done for 8 h. The spark plasma compaction was done using the FCT Systeme HP D 10 device with a heating rate of 200 °C/min until reaching the compaction temperature of 1000 °C. The compacted powder was then compressed with a pressure of 48 MPa, remaining compressed for another 9 minutes followed by rapid cooling. The chemical (XRF) and phase compositions (XRD) were determined using the ARL 9400 XP and PANalytical X'Pert Pro (Cu $K_{\alpha 1}$ λ=1,54059·10^{-10} m) devices. Prepared compact samples were ground on SiC abrasive papers P180-P2500 and polished using a diamond paste. For the microstructural observations, the samples were etched in an aqua regia (mixture of HNO_3 and HCl in a ratio of 1:3). Such samples were then investigated for microstructure before being exposed to corrosion tests. Then they were again ground and polished to diminish the influence of etching. Potentiodynamic corrosion testing in a physiologic solution (9 g/l NaCl) tempered at 37 °C was done using a three-electrode Gamry PCI4 potentiostat combining Pt wire as counter electrode and Ag/AgCl (ACLE) reference electrode. The open circuit potential (EOC) was stabilized for 3600 s, and the polarization resistance (Rp) was measured within ± 0.2 V/EOC with a scanning speed of 0.125 mV/s. Potentiodynamic anode curves (PDA) were measured within the range of -0.05 V/EOC up to 1 V/ACLE with a scanning speed of 1 mV/s. The prepared compact samples were compared with the corrosion behaviour of the 316L stainless steel, which is commonly used in medicinal applications, mostly as implants. The Atomic Force Microscopy together with Scanning Kelvin Probe Microscopy (AFM-SKPM) using the AIST-NT Inc. SmartSPM 1000 device were employed to describe the correlation between the surface quality, phase distribution and corrosion performance while being tested in the physiological solution. The prepared compacts were also subjected to long-term annealing at 600 °C to determine their resistance against high-temperature oxidation. For this purpose, larger specimens were put into Al_2O_3 annealing crucibles and put into the electric resistance furnace for time intervals 1, 2.5, 5, 7.5, 10, 20, 40, 60, 80 and 100h to determine the oxidation kinetics. The crucibles were at each particular time segment removed from the furnace and cooled down to laboratory temperature being covered by an Al_2O_3 lid and then, the sample was weighed for oxide gains. It should be noted, that these lids were not present during the annealing itself, to avoid any possible effect on the oxidation kinetics due to unequal conditions for individual samples.

3 Results and discussion

3.1 Chemical, phase and microstructure composition

The results of the chemical composition of prepared MA+SPS alloys determined by the XRF analysis are shown in Fig. 1. It is obvious, that the concentration of Fe is increasing since the hardness of the initial elements changes due to the formation of new phases. The phase formation is accompanied by an instantaneous hardness increase compared to the initial powder mixture. This results in increased wear of the milling elements and the jar itself, increasing the contamination by the elements of the jar (mainly Fe) in all of the prepared alloys. On the other hand, the content of the rest of the elements was therefore lowered at the expense of increasing Fe content. In addition, some of the pure elements could get stuck in the corners of the jar, especially when considering the fine nature of the powders used for MA.

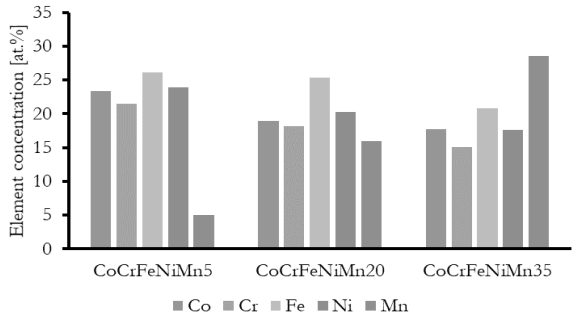

Fig. 1 *Chemical composition (at.%) of prepared MA+SPS compact alloys determined by the XRF analysis*

The prepared powders and compact samples were investigated for the phase compositions as shown in Fig. 2. As it was discovered, the phase compositions and their content within the alloys did not change with increasing content of Mn. Moreover, the phase composition was identical to those of powders before being compacted (not shown). The present phases were identified as FCC $Mn_{0.25}Fe_{0.5}Ni_{0.25}$ and as a smaller fraction of orthorhombic carbides matched with Cr_7C_3. More importantly, the values of the lattice parameter d of the FCC phase changed accordingly to the content of Mn starting at 0.20663 nm (Mn5 alloy) and steadily increasing to 0.20728 (Mn20) until reaching the highest value of 0.20841 nm (for Mn35 alloy). The change in the lattice parameter of the FCC phase documents the increasing content of Mn within it, which may be associated with the increasing content of Mn, which has slightly higher atomic radii compared to the rest elements.

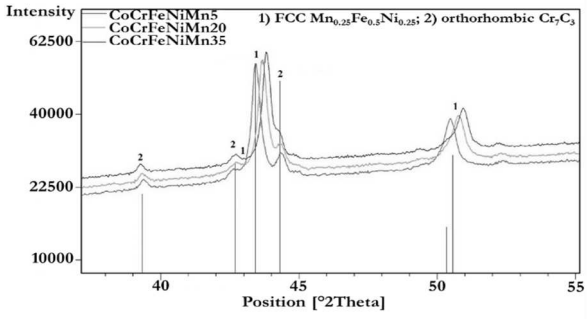

Fig. 2 *XRD patterns of the MA+SPS compact alloys*

Additionally, the full width at half maximum values of the most intensive peaks of FCC solid solution either the powders or the compacts found around 43.5° were compared as is shown in Tab. 1. Initially, the powder shows significantly higher FWHM values suggesting the significant microstructural refinement and also a lattice stress-strain. These values significantly decreases during the SPS compaction which is related to the microstructural refinement and partial relaxation of the stresses within the crystallographic lattice. The first of the aforementioned effects was probably responsible for the most significant reduction of the FWHM value of Mn5 alloy from 0.662 to 0.252. As the HEAs are known to be highly thermallly stable due to strongly limited diffusion processes due to the high value of configurational entropy, reducing content of one of five elements that are forming the solid solution down to only 5 at.% is responsible for increasing the diffusivity of other elements within the alloy. On the other hand, the rest of the alloys showed significantly lower decrease of the FWHM value which can be associated to the their higher thermal stability and therefore resistence against diffussion-related efects including the microstructural coarsening and also lattice realaxations.

Tab. 1 *Change of the average FWHM values for the most intensive peaks of FCC solid solutions*

Alloy	Average FWHM values	
	MA powder	MA+SPS
CoCrNiFeMn5	0.662	0.252
CoCrNiFeMn20	0.500	0.262
CoCrNiFeMn35	0.413	0.230

The light micrographs of the prepared compact alloys are shown in Fig. 3. As is shown, the microstructure was in the case of all the alloys composed of sub-micrometre phases with the presence of small pores, manifesting themselves as randomly distributed circular black spots. The formation of these pores is due to Cl^- ions which are known for localized corrosion attacks and dissolution on a variety of materials. Small grey areas may correspond to the presence of carbides identified as orthorhombic Cr_7C_3, which are known to possess a high hardness of approximately 1380 HV [11], thus significantly hardening the alloy. On the other hand, these carbides are the reason for the high potential difference within the alloy, which might cause the formation of distinctive anodic/cathodic areas resulting in uneven corrosion.

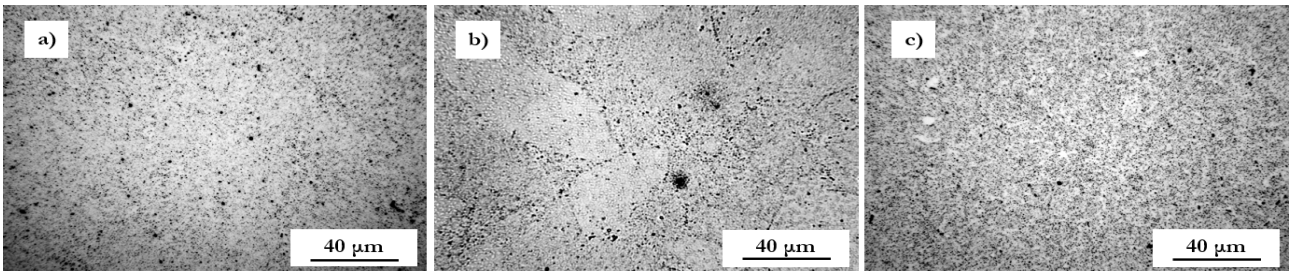

Fig. 3 *LM micrographs of the compacts after being etched*

3.2 Corrossion behaviour in aqaueous and dry conditions

3.2.1 Exposure to physiological solution

The prepared alloys were tested in a physiological solution to determine their basic behaviour and to evaluate their ability to be used as biomaterials before being further investigated using way advanced testing, e.q. in SBF solutions for the cytotoxicity. For this purpose, the 3-electrode potentiodynamic measurements were done in an electrochemical corrosion cell, with the specimen serving as the bottom of the cell to describe the behaviour of prepared alloys in wet conditions. The corrosion behaviour of all the tested alloys and also of the reference 316L stainless steel are shown in Fig. 4, while the results are summarized in Tab. 2.

Accordingly, to the results, it is obvious that the lowest corrosion current density i_{corr} of 0.13 μA/cm² in the physiologic solution is achieved for the 316L steel. More importantly, the data shows the creation of either a passive or barrier layer on the 316L surface during the polarization which is stable until a breakthrough potential E_b of 35.4 mV/ACLE. In comparison, the prepared Mn HEAs showed a bit lower corrosion resistance which increased with the content of Mn within the alloy. That means the corrosion speed increased with the Mn content while the open circuit potential (EOC) shifted to more negative values. The icorr of the Mn35 alloy was approximately 10-times higher compared to the reference 316L steel (see Tab. 3). This behaviour is similar to the observations of Zhang et al. [9], confirming the negative effect of the Mn on the corrosion resistance of the CoCrFeNi-based alloy. On the other hand, both the Mn5 and Mn20 alloys were showing the formation of a barrier layer that was stable up to E_b of -105.0 and -191.3 mV/ACLE, respectively. The presence of the barrier layer is favoured due to a relatively high current density (see Fig. 4). On the other hand, the Mn35 alloy did not show similar behaviour since it corroded in activity during the whole exposition (Fig. 4).

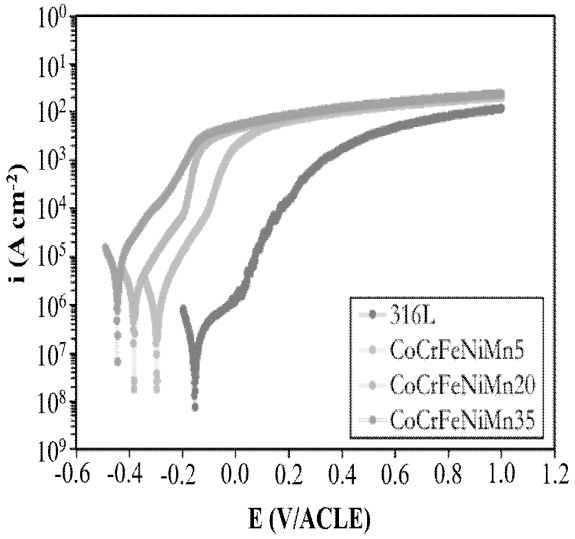

Fig. 4 *Potentiodynamic anode curves (PDA) of the studied HEA alloys and the 316L reference in physiologic solution at 37 °C*

Tab. 2 *Results of the electrochemical testing of the reference 316 L steel and the MA+SPS alloys*

Alloy	EOC(mV/ACLE)	R_p(Ωm²)	i_{corr}(μA/cm²)	E_b(mV/ACLE)
316 L	-147.5	9.3	0.13	35.4
CoCrFeNiMn5	-219.9	1.5	0.66	-105.0
CoCrNiFeMn20	-375.0	0.8	1.41	-191.3
CoCrNiFeMn35	-440.3	0.3	6.34	-

The SEM+EDS element distribution maps after the electrochemical testing show an uneven distribution of elements across the exposed surface, confirming an uneven dissolution due to the formation of anodic/cathodic areas. This can be directly matched with the AFM-SKPM measurements, which showed the presence of unevenly distributed particles, accordingly to the topography measurements, emerging from the polished surface. This corresponds to the presumption that these particles shall be significantly harder than the rest of the material that underwent a more pronounced mass loss during polishing.

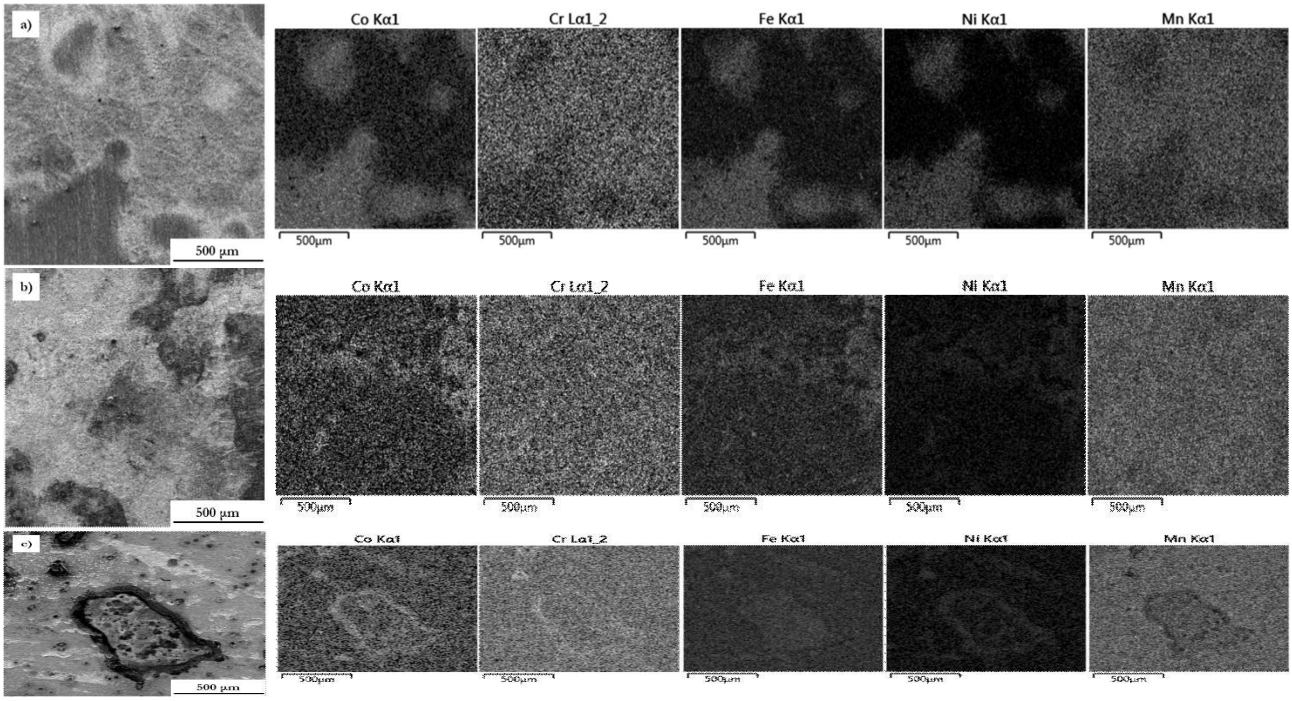

Fig. 5 *The SEM+EDS element distribution maps on the surface of the: a) CoCrFeNiMn5; b) CoCrFeNiMn20; c) CoCrFeNiMn35 alloy after the electrochemical testing*

This prediction has been also confirmed by the SKPM measurements, showing a potential difference reaching up to 60 mV compared to the rest of the alloy matrix (Fig. 6). Considering both the above mentioned, the presence of Cr-based carbides was also reported in the work of Thurlova et al. [2]. The dimensions of present carbides increase with the content of Mn, forming more dense clusters acting as cathodic areas within the metallic matrix. On the other hand, the increasing content of Mn within the alloy did not significantly increase the FCC lattice stress accordingly to the FWHM values (see Tab. 1), since it tends to segregate on the sub-grain boundaries accelerating the diffusion paths [12]. This results in a rapid formation of Cr-rich regions, resulting further in systems containing C, into the formation of carbides. Moreover, these carbides are known for the mutual substitution of Cr by other elements having similar or even slightly lower atomic radii.

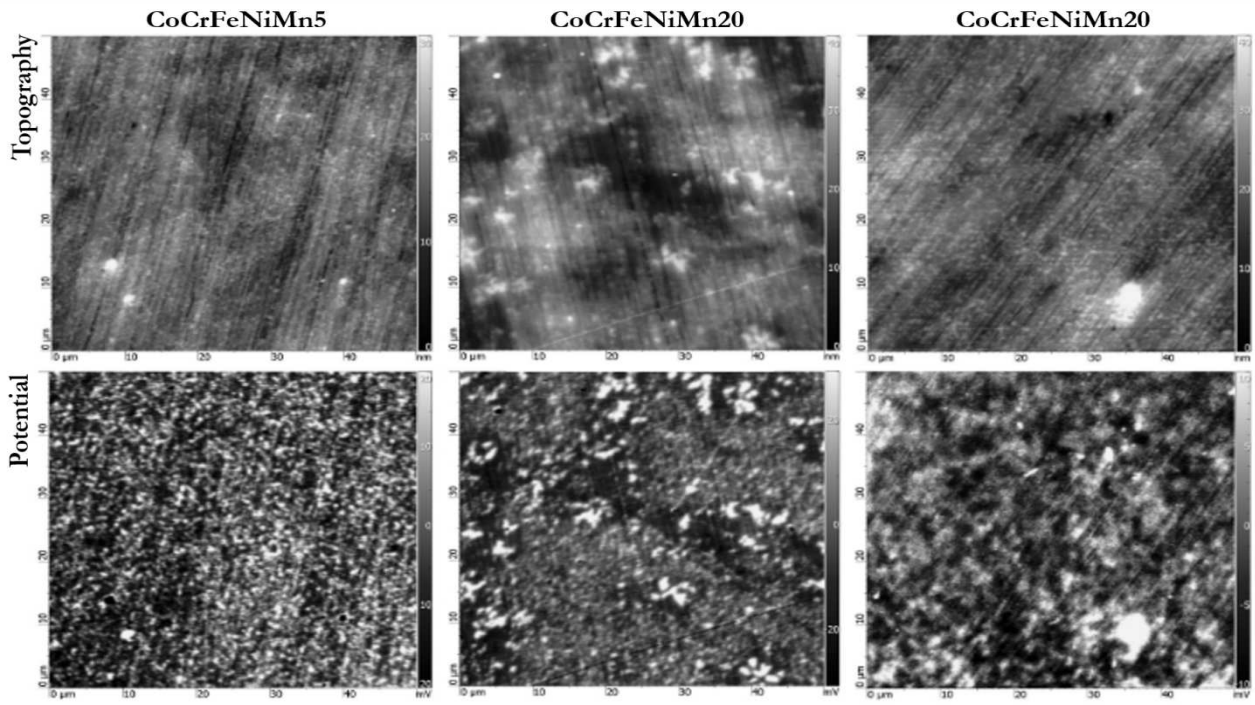

Fig. 6 *AFM-SKPM maps of the surface of prepared compacts showing the topology and corresponding potential differences*

3.2.2 Exposure to elevated temperature

The prepared MA+SPS compacts were also subjected to long-term annealing at an elevated temperature of 600 °C to determine their resistance against oxidation. As is shown in Tab. 3, the compacts were showing slightly different behaviour, which can be briefly accompanied by the overall content of Mn within the alloy. As is shown, the lower the content of Mn, the better the resistance of the alloy against oxidation. Increasing the content of Mn up to 20 at.%, the alloy starts to become less oxidation resistant increasing the total amount of the newly formed weighing up to 0.0016g. Exceeding the 20 at.% of Mn results in intensive delamination of flaky-like oxide products resulting in weight loss of 0.0012g.

Tab. 3 *The weight gain of the CoCrFeNiMnX (X=5, 20 and 35 at.%) alloy during 100h annealing at 600 °C*

Alloy	Weight change after 100h at 600 °C (g)		
	m_0	m_{100}	Δm
CoCrNiFeMn5	0.4952	0.4955	**0.0003**
CoCrNiFeMn20	0.4806	0.4822	**0.0016**
CoCrNiFeMn35	0.5111	0.5099	**-0.0012**

This behaviour corresponds to the observations of the surface after 100 h of annealing as is shown in Fig. 7. One can see, that the appearance corresponds to the weight change measurements confirming the negative effect of the Mn content. As the Mn content is low, the oxide layer is non-evenly distributed, and its growth is site-preferred with only an occasional occurrence of layer delamination. On the other hand, the CoCrFeNiMn20 alloy showed the most compact oxide layer among all the tested alloys without any significant traces of delamination. This was the main cause for reaching the highest weight gains over the tested period. Further increase in the Mn content resulted in the heavy flaking of the oxides into specks. The amount of the delaminated oxides across all the compacts could not be precisely determined since they flew out of the annealing crucibles into the furnace's inner space, mostly during their re-insertion after being weighed. This also confirms the relatively bad protective performance due to high thermally-induced stresses within the oxide layer caused by the thermal cycling programme. Nevertheless, except for the oxide delamination and their poor protective ability, the overall oxidation speed seemed to be quite slow, although the character of the oxidic layer is far from ideal. This can be caused by the depletion of Mn from the sub-surface areas slowing down the overall oxidation speed.

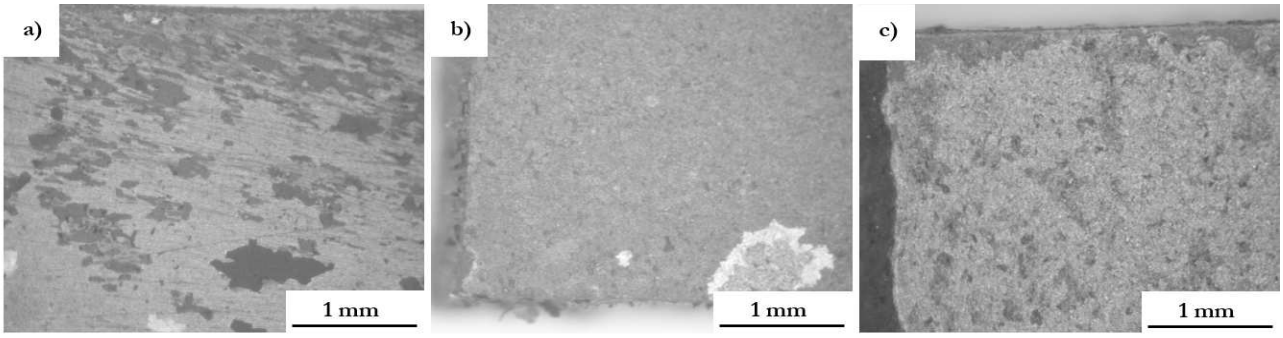

Fig. 7 *The surface appearance of the: a) CoCrFeNiMn5; b) CoCrFeNiMn20; c) CoCrFeNiMn35compacts after being exposed for 100 h at 600 °C*

4 Conclusion

The CoCrFeNiMnX (X=5, 20 and 35 at.%) were successfully prepared by the combination of mechanical alloying and compacted via spark plasma sintering. As was shown, the chemical composition slightly differed from those initially targeted, which is typical for mechanical alloying processes. However, the phase composition did not change accordingly to the content of Mn, being identified as FCC solid solution and a mixture of Cr-based carbides. Considering the corrosion resistance, the higher the Mn content within the alloy, the higher the i_{corr} and the more the EOC shifts towards more negative values. The AFM-SKPF measurements also provided a clearly distinguished presence of areas identified as Cr_7C_3, showing potential differences reaching up to 60 mV. Moreover, their overall dimensions increased with the content of Mn within the HEA forming bulky areas supporting uneven corrosion due to the formation of anodic/cathodic areas. During the dry corrosion, the tested HEAs showed a formation of an oxide layer that was heavily delaminated due to thermal shocks. Among the variety of tested contents of Mn, the equiatomic CoCrFeNiMn alloy showed the most compact layer that did not heavily delaminate compared to the rest of the tested alloys.

Acknowledgement

This research was financially supported by Czech Science Foundation (grant No. 21-11313S).

References

[1] ČECH, J.; HAUŠILD, P.; KARLÍK, M.; ČAPEK, J., and PRŮŠA, F. Indentation Size

Effect in CoCrFeMnNi HEA Prepared by Various Techniques. *Materials* 2021, 14 (23), 7246

[2] THÜRLOVÁ, H. and PRŮŠA, F. Influence of the Al Content on the Properties of Mechanically Alloyed CoCrFeNiMnXAl20−X High-Entropy Alloys. *Materials* 2022, 15 (22)

[3] KRATOCHVÍL, P. and PRŮŠA, F. CoCrFeNiTi High Entropy Alloy Prepared via Mechanical Alloying and Spark Plasma Sintering. *Manufacturing Technology,* 2022, 22 (4), 423-428

[4] STRAKOSOVA, A.; KRATOCHVÍL, P.; RIEDL, J., and PRŮŠA, F. Phase and Mechanical Properties Response of the Mechanically Alloyed CoCrFeNiAlX High Entropy Alloys. *Manufacturing Technology*, 2022, 22 (4), 471-476

[5] THÜRLOVÁ, H. and PRŮŠA, F. Partial Substitution of Mn by Al in the Cocrfenimnxal20-X (X=5, 10, 15) High Entropy Alloy Prepared of Mechanical Alloying and Spark Plasma Sintering. *Manufacturing Technology,* 2022, 22 (3), 342-346

[6] PRŮŠA, F.; CABIBBO, M.; ŠENKOVÁ, A.; KUČERA, V.; VESELKA, Z.; ŠKOLÁKOVÁ, A.; VOJTĚCH, D.; CIBULKOVÁ, J., and ČAPEK, J. High-strength ultrafine-grained CoCrFeNiNb high-entropy alloy prepared by mechanical alloying: Properties and strengthening mechanism. *Journal of Alloys and Compounds* 2020, 835 155308

[7] PRUŠA, F.; ŠENKOVÁ, A.; VOJTECH, D.; CAPEK, J., and BERNATIKOVÁ, A. High entropy alloys prepared by combination of mechanical alloying and spark plasma sintering. *Manufacturing Technology*, 2016, 16 (6), 1350-1354.

[8] GAO, P.-H.; FU, R.-T.; CHEN, B.-Y.; ZENG, S.-C.; ZHANG, B.; YANG, Z.; GUO, Y.-C.; LIANG, M.-X.; LI, J.-P.; LU, Y.-Q.; JIA, L., and ZHAO, D. Corrosion Resistance of CoCrFeNiMn High Entropy Alloy Coating Prepared through Plasma Transfer Arc Claddings. *Metals* 2021, 11 (11), 1876

[9] ZHANG, C.; ZHU, M.; YUAN, Y., and GUO, S. The effect of Mn addition on corrosion behaviour of equiatomic CoCrFeNi high entropy alloys in NaCl solution. Corrosion Engineering, *Science and Technology* 2022, 1-11

[10] TIAN, Y.; LU, C.; SHEN, Y., and FENG, X. Microstructure and corrosion property of CrMnFeCoNi high entropy alloy coating on Q235 substrate via mechanical alloying method. *Surfaces and Interfaces* 2019, 15 135-140

[11] SUN, L.; JI, X.; ZHAO, L.; ZHAI, W.; XU, L.; DONG, H.; LIU, Y., and PENG, J. First Principles Investigation of Binary Chromium Carbides Cr7C3, Cr3C2 and Cr23C6: Electronic Structures, Mechanical Properties and Thermodynamic Properties under Pressure. *Materials* 2022, 15 (2), 558

[12] ZHANG, Y.; BIAN, T.; SHEN, X.; WANG, Z.; YE, S.; FENG, S.; YU, K.; DING, C., and YU, P. Sintering mechanism and microstructure evolution of a CoCrFeNiMn high entropy alloy fabricated by metal injection molding. *Journal of Alloys and Compounds* 2021, 868 158711